J|A|C|S ARTICLES

Published on Web 03/24/2010

Roles of the Distinct Electronic Structures of the $\{Fe(NO)_2\}^9$ and $\{Fe(NO)_2\}^{10}$ Dinitrosyliron Complexes in Modulating Nitrite Binding Modes and Nitrite Activation Pathways

Fu-Te Tsai, Pei-Lin Chen, and Wen-Feng Liaw*

Department of Chemistry, National Tsing Hua University, Hsinchu 30013, Taiwan

Received January 31, 2010; E-mail: wfliaw@mx.nthu.edu.tw

Abstract: Nitrosylation of $[PPN]_2[(ONO)_2Fe(\eta^2\text{-}ONO)_2]$ [**1**; PPN = bis(triphenylphosphoranylidene)-ammonium] yields the nitrite-containing $\{Fe(NO)\}^7$ mononitrosyliron complex (MNIC) $[PPN]_2[(NO)Fe(ONO)_3(\eta^2\text{-}ONO)]$ (**2**). At 4 K, complex **2** exhibits an $S = {}^3/_2$ axial EPR spectrum with principal g values of $g_\perp = 3.971$ and $g_\parallel = 2.000$, suggestive of the $\{Fe^{III}(NO^-)\}^7$ electronic structure. Addition of 1 equiv of PPh_3 to complex **2** triggers O-atom transfer of the chelating nitrito ligand under mild conditions to yield the $\{Fe(NO)_2\}^9$ dinitrosyliron complex (DNIC) $[PPN][(ONO)_2Fe(NO)_2]$ (**3**). These results demonstrate that both electronic structure [$\{Fe^{III}(NO^-)\}^7$, $S = {}^3/_2$] and redox-active ligands ($[RS]^-$ for $[(RS)_3Fe(NO)]^-$ and $[NO^-]$ for complex **2**) are required for the transformation of $\{Fe(NO)\}^7$ MNICs into $\{Fe(NO)_2\}^9$ DNICs. In comparison with the PPh_3-triggered O-atom abstraction of the chelating nitrito ligand of the $\{Fe(NO)_2\}^9$ DNIC $[(1\text{-MeIm})_2(\eta^2\text{-}ONO)Fe(NO)_2]$ (**5**; 1-MeIm = 1-methylimidazole) to generate the $\{Fe(NO)_2\}^{10}$ DNIC $[(1\text{-MeIm})(PPh_3)Fe(NO)_2]$ (**6**), glacial acetic acid protonation of the N-bound nitro ligand in the $\{Fe(NO)_2\}^{10}$ DNIC $[PPN][(\eta^1\text{-}NO_2)(PPh_3)Fe(NO)_2]$ (**7**) produced the $\{Fe(NO)_2\}^9$ DNIC $[PPN][(OAc)_2Fe(NO)_2]$ (**8**), nitric oxide, and H_2O. These results demonstrate that the distinct electronic structures of $\{Fe(NO)_2\}^{9/10}$ motifs [$\{Fe(NO)_2\}^9$ vs $\{Fe(NO)_2\}^{10}$] play crucial roles in modulating nitrite binding modes (O-bound chelating/monodentate nitrito for $\{Fe(NO)_2\}^9$ DNICs vs N-bound nitro as a π acceptor for $\{Fe(NO)_2\}^{10}$ DNICs) and regulating nitrite activation pathways (O-atom abstraction by PPh_3 leading to the intermediate with a nitroxyl-coordinated ligand vs protonation accompanied by dehydration leading to the intermediate with a nitrosonium-coordinated ligand). That is, the redox shuttling between the $\{Fe(NO)_2\}^9$ and $\{Fe(NO)_2\}^{10}$ DNICs modulates the nitrite binding modes and then triggers nitrite activation to generate nitric oxide.

Introduction

Dinitrosyliron complexes (DNICs) are known to act as the intrinsic NO-derived species that appear in various NO-producing tissues.[1a,b] The binding of NO to [Fe−S] cluster-containing proteins or enzymes in mitochondria to give DNICs and dinuclear $[Fe(\mu\text{-}SR)(NO)_2]_2$ (Roussin's red ester) has been intensely studied.[1c,d] Also, nitrosylation of the chelatable iron pool (CIP) to produce paramagnetic protein-bound DNICs has been demonstrated.[1e,f] DNICs are known to be one of the possible forms for storage and transport of NO in biological systems. Nitric oxide in vivo can be stabilized and stored in the form of DNICs with proteins (protein-bound DNICs) and is probably released from cells in the form of low-molecular-weight DNICs (LMW-DNICs).[2] Characterization of both protein-bound DNICs and LMW-DNICs in vitro is known to be via their distinct EPR signals at an average g value of 2.03.[2]

Nitrite, an ubiquitous endocrine molecule, has been known to serve as an intravascular NO storage and transport species to transduce NO bioactivity in blood circulation.[3] The plasma nitrite level in human beings was measured to be in the range 50−300 nM.[3a,e] Nitrite signaling operates through cooperation with hemes, thiols, amines, polyphenols, and ascorbate, yielding nitric oxide, *S*-nitrosothiols, *N*-nitrosamines, and iron nitrosyl complexes during physiological and pathological hypoxia, respectively.[3a] Systematic nitric oxide synthase (NOS)-independent NO formation from nitrite reduction was first demonstrated in the ischemic heart, showing that nitrite-mediated cytoprotection appears to be NO-dependent and mitochondria-

(1) (a) Mülsch, A.; Mordvintcev, P. I.; Vanin, A. F.; Busse, R. *FEBS Lett.* **1991**, *294*, 252–256. (b) Henry, Y.; Lepoivre, M.; Drapier, J. C.; Ducrocq, C.; Boucher, J. L.; Guissani, A. *FASEB J.* **1993**, *7*, 1124–1134. (c) Foster, M. W.; Cowan, J. A. *J. Am. Chem. Soc.* **1999**, *121*, 4093–4100. (d) Kennedy, M. C.; Antholine, W. E.; Beinert, H. *J. Biol. Chem.* **1997**, *272*, 20340–20347. (e) Toledo, J. C., Jr.; Bosworth, C. A.; Hennon, S. W.; Mahtani, H. A.; Bergonia, H. A.; Lancaster, J. R., Jr. *J. Biol. Chem.* **2008**, *283*, 28926–28933. (f) Lewandowska, H.; Meczyńska, S.; Sochanowicz, B.; Sadło, J.; Kruszewski, M. *J. Biol. Inorg. Chem.* **2007**, *12*, 345–352.

(2) (a) Szaciłowski, K.; Chmura, A.; Stasicka, Z. *Coord. Chem. Rev.* **2005**, *249*, 2408–2436. (b) McCleverty, J. A. *Chem. Rev.* **2004**, *104*, 403–418. (c) Butler, A. R.; Megson, I. L. *Chem. Rev.* **2002**, *102*, 1155–1165. (d) Boese, M.; Keese, M. A.; Becker, K.; Busse, R.; Mülsch, A. *J. Biol. Chem.* **1997**, *272*, 21767–21773. (e) Boese, M.; Mordvintcev, P. I.; Vanin, A. F.; Busse, R.; Mulsch, A. *J. Biol. Chem.* **1995**, *270*, 29244–29249. (f) Lee, M.; Arosio, P.; Cozzi, A.; Chasteen, N. D. *Biochemistry* **1994**, *33*, 3679–3687.

(3) (a) Lundberg, J. O.; Weitzberg, E.; Gladwin, M. T. *Nat. Rev. Drug Discovery* **2008**, *7*, 156–167. (b) Bryan, N. S.; Fernandez, B. O.; Bauer, S. M.; Garcia-Saura, M. F.; Milsom, A. B.; Rassaf, T.; Maloney, R. E.; Bharti, A.; Rodriguez, J.; Feelish, M. *Nat. Chem. Biol.* **2005**, *1*, 290–297. (c) Gladwin, M. T. *Nat. Chem. Biol.* **2005**, *1*, 245–246. (d) Cosby, K.; et al. *Nat. Med.* **2003**, *9*, 1498–1505. (e) Gladwin, M. T.; Shelhamer, J. H.; Schechter, A. N.; Pease-Fye, M. E.; Waclawiw, M. A.; Panza, J. A.; Ognibene, F. P.; Cannon, R. O., III. *Proc. Natl. Acad. Sci. U.S.A.* **2000**, *97*, 11482–11487.

10.1021/ja100849r

targeted.[3a] Nitrite-dependent NO formation can modulate inflammation, drive cGMP-dependent signaling under hypoxic stress, and inhibit the formation of mitochondrial-derived reactive oxygen species (ROS).[3] Recently, it was demonstrated that nitrite, one of the bioactive metabolic intermediates of nitroglycerin (GTN) biotransformation in vascular smooth muscle cells, is relevant to hypoxic vasodilation, which alleviates chest pain experienced by patients suffering from angina pectoris, heart failure, and myocardial infarction.[4]

In nitrite activation triggered by iron complexes, the interconversion between [(TpivPP)Fe(III)(NO_2)(Py)] containing a N-bound nitro ligand and the {Fe(NO)}^{7} mononitrosyliron complex (MNIC) [(TpivPP)Fe(NO)] was demonstrated upon addition of PPh_3 and O_2−pyridine, respectively, in $CHCl_3$.[5] To understand the catalytic mechanism of cytochrome cd_1 nitrite reductase (NIR), the five-coordinate {Fe(NO)}^{6} [(CTPP)Fe(NO)] complex was generated via protonation (intramolecular proton transfer) of [(HCTPPH)Fe(II)−NO_2].[6] Recently, Mascharak and co-workers[7] demonstrated that the non-heme complex [($PaPy_3$)Fe−NO_2][ClO_4] containing a N-bound nitro ligand and the {Fe(NO)}^{7} MNIC [($PaPy_3$)Fe(NO)][ClO_4] are chemically interconvertable in the presence of PPh_3 and O_2, respectively. In the Cu-NIR model study reported by Tolman and coworkers,[8] the synthetic Cu(I)−nitro complex [(TACN)Cu−NO_2] containing a N-bound nitro ligand was converted into NO(g) via a putative {Cu(NO)}^{10} intermediate in the presence of 2 equiv of acetic acid. In our previous report, the temperature-dependent dynamic equilibrium between the six-coordinate {Fe(NO_2)$_2$}^{9} octahedral DNIC [(1-MeIm)$_2$(η^2-ONO)Fe(NO_2)$_2$] (**5**; 1-MeIm = 1-methylimidazole) (g = 2.013) and the four-coordinate {Fe(NO_2)$_2$}^{9} tetrahedral DNIC [(1-MeIm)(ONO)Fe(NO_2)$_2$] (**4**) (g = 2.03) was demonstrated.[9] Also, the chelating nitrito ligand of the six-coordinate {Fe(NO_2)$_2$}^{9} DNIC [(1-MeIm)$_2$(η^2-ONO)Fe(NO_2)$_2$] undergoes PPh_3-triggered O-atom transfer, affording NO(g) and the {Fe(NO_2)$_2$}^{10} DNIC [(1-MeIm)(PPh_3)Fe(NO_2)$_2$] (**6**).[9] In the present work, the synthesis of the O-bound monodentate/bidentate nitrito complex [PPN]$_2$[(ONO)$_2$Fe(η^2-ONO)$_2$] [**1**; PPN = bis(triphenylphosphoranylidene)ammonium], nitrosylation of complex **1** to afford the MNIC [PPN]$_2$[(ONO)$_3$Fe(NO)(η^2-ONO)] (**2**), and transformation of MNIC **2** into the {Fe(NO_2)$_2$}^{9} DNIC [PPN][(ONO)$_2$Fe(NO_2)$_2$] (**3**) are demonstrated. In particular, the possible roles for {Fe(NO)}^{7}/{Fe(NO_2)$_2$}^{10} motifs in modulating nitrite activation [i.e., O-atom abstraction of the O-bound nitrito ligand in the {Fe(NO)}^{7} MNIC **2** by PPh_3 to generate the {Fe(NO_2)$_2$}^{9} DNIC [PPN][(ONO)$_2$Fe(NO_2)$_2$] (**3**) along with $OPPh_3$ vs protonation of the N-bound nitro ligand in the {Fe(NO_2)$_2$}^{10} DNIC [PPN][(η^1-NO_2)(PPh_3)Fe(NO_2)$_2$] (**7**) to produce the {Fe(NO_2)$_2$}^{9} DNIC [PPN][(OAc)$_2$Fe(NO_2)$_2$] (**8**) accompanied by release of NO(g)] are also reported.

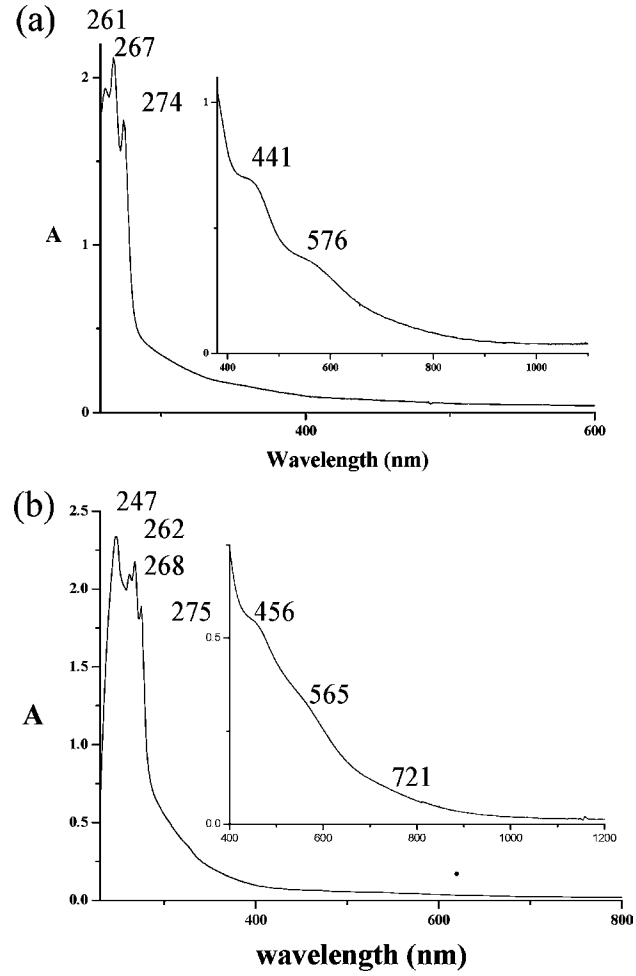

Figure 1. UV−vis spectra of (a) complex **1** in CH_3CN at 233 K and (b) complex **2** in CH_2Cl_2 at 300 K.

Results and Discussion

Synthesis of Complex 1 and Transformation of Nitrite to Nitric Oxide Activated by {Fe(NO)}^{7} MNIC 2 via a Nitroxyl-Containing Intermediate. Reaction of ferrous chloride with $AgNO_2$ and [PPN][NO_2] (1:2:2 molar ratio) in CH_3CN at 0 °C yielded the thermally unstable, dark-yellow-brown complex [PPN]$_2$[(ONO)$_2$Fe(η^2-ONO)$_2$] (**1**) (38% yield) bearing two chelating O-bound nitrito ligands and two monodentate O-bound nitrito ligands. Complex **1** was characterized by single-crystal X-ray diffraction and UV−vis spectroscopy. The UV−vis spectrum of complex **1** in CH_3CN displays absorptions at 261, 267, 274, 441, and 576 nm at 233 K (Figure 1a). Upon injection of NO gas (10% NO + 90% N_2) into a CH_3CN solution of complex **1** at 0 °C, a rapid reaction ensued over the course of 5 min to give the dark-red-brown chelating nitrito-containing {Fe(NO)}^{7} MNIC [PPN]$_2$[(ONO)$_3$Fe(NO)(η^2-ONO)] (**2**), which was characterized by IR [ν_{NO} (cm^{-1}): 1777(s) (THF); 1800(s) (CH_2Cl_2); 1768(s) (KBr)], electron paramagnetic resonance

(4) (a) Ignarro, L. J. *Proc. Natl. Acad. Sci. U.S.A.* **2002**, *99*, 7816–7817. (b) Zhiqiang, C.; Zhang, J.; Stamler, J. S. *Proc. Natl. Acad. Sci. U.S.A.* **2002**, *99*, 8306–8311. (c) Wenzel, P.; Hink, U.; Oelze, M.; Schuppan, S.; Schaeuble, K.; Schildknecht, S.; Ho, K. K.; Weiner, H.; Bachschmid, M.; Münzel, T.; Daiber, A. *J. Biol. Chem.* **2007**, *282*, 792–799. (d) Artz, J. D.; Toader, V.; Zavorin, S. I.; Bennett, B. M.; Thatcher, G. R. J. *Biochemistry* **2001**, *40*, 9256–9264.
(5) Cheng, L.; Powell, D. R.; Khan, M. A.; Richter-Addo, G. B. *Chem. Commun.* **2000**, 2301–2302.
(6) (a) Einsle, O.; Messerschmidt, A.; Huber, R.; Kroneck, P. M. H.; Neese, F. *J. Am. Chem. Soc.* **2002**, *124*, 11737–11745. (b) Ching, W.-M.; Chuang, C.-H.; Wu, C.-W.; Peng, C.-H.; Hung, C.-H. *J. Am. Chem. Soc.* **2009**, *131*, 7952–7953.
(7) (a) Patra, A. K.; Afshar, R. K.; Rowland, J. M.; Olmstead, M. M.; Mascharak, P. K. *Angew. Chem.* **2003**, *115*, 4655–4659. (b) Afshar, R. K.; Eroy-Reveles, A. A.; Olmstead, M. M.; Mascharak, P. K. *Inorg. Chem.* **2006**, *45*, 10347–10354.
(8) (a) Halfen, J. A.; Mahapatra, S.; Olmstead, M. M.; Tolman, W. B. *J. Am. Chem. Soc.* **1994**, *116*, 2173–2174. (b) Halfen, J. A.; Tolman, W. B. *J. Am. Chem. Soc.* **1994**, *116*, 5475–5476. (c) Halfen, J. A.; Mahapatra, S.; Wilkinson, E. C.; Gengenbach, A. J.; Young, V. G., Jr.; Que, L., Jr.; Tolman, W. B. *J. Am. Chem. Soc.* **1996**, *118*, 763–776.
(9) Tsai, F.-T.; Kuo, T.-S.; Liaw, W.-F. *J. Am. Chem. Soc.* **2009**, *131*, 3426–3427.

Scheme 1

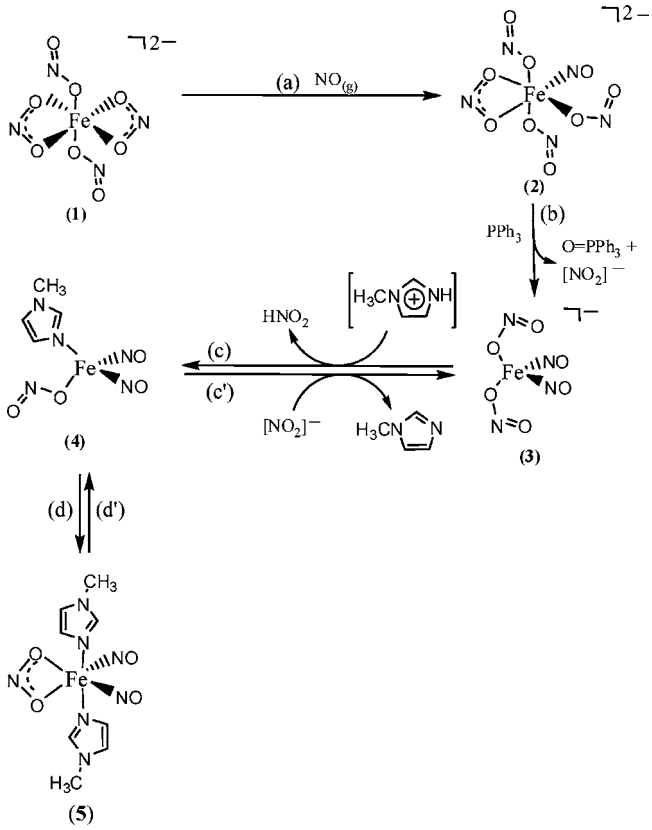

(EPR), and UV−vis spectroscopy as well as single-crystal X-ray crystallography (Scheme 1a). The higher NO stretching frequency of complex **2** may be ascribed to the weak electron-donating ability of O-bound nitrito ligands.[10] At 4 K, complex **2** exhibits an $S = {}^3/_2$ axial EPR spectrum with principal g values of $g_\perp = 3.971$ and $g_\parallel = 2.000$ (Figure 2), suggestive of the $\{Fe^{III}(NO^-)\}^7$ electronic structure.[10] The UV−vis spectrum of complex **2** in CH_2Cl_2 exhibits absorptions at 247, 262, 268, 275, 456, 565, and 721 nm (Figure 1b). The net molar magnetic susceptibility (χ_M) of complex **2** increases from 7.040×10^{-3} cm^3 mol^{-1} at 300 K to 0.654 cm^3 mol^{-1} at 2 K. The corresponding $\chi_M T$ values (2.110 cm^3 mol^{-1} K at 300 K) and effective magnetic moments ($\mu_{eff} = 4.111\mu_B$ at 300 K) exhibit temperature-independent magnetic behavior indicating that the ground state is $S_{total} = {}^3/_2$ (Figure S1 in the Supporting Information).

In the previous communication,[9] we demonstrated that the $\{Fe(NO)_2\}^9$ DNICs [(1-MeIm)(ONO)Fe$(NO)_2$] (**4**) and [(1-MeIm)$_2$(η^2-ONO)Fe$(NO)_2$] (**5**) are interconvertable and that the chelating nitrito ligand of **5** undergoes PPh_3-triggered O-atom transfer that results in reductive elimination of NO along with the production of the $\{Fe(NO)_2\}^{10}$ DNIC [(1-MeIm)(PPh_3)Fe$(NO)_2$] (**6**). As shown in Scheme 1b, addition of 1 equiv of PPh_3 to complex **2** was presumed to trigger O-atom transfer from the chelating nitrito ligand under mild conditions to yield $OPPh_3$ (^{31}P NMR: $\delta = 30.4$ ppm in $CDCl_3$)[7] and the known $\{Fe(NO)_2\}^9$ DNIC [PPN][(ONO)$_2$Fe$(NO)_2$] (**3**) via the proposed intermediate $[(ONO)_3Fe^{III}(NO^-)_2]^{2-}$ along with elimination of [PPN][NO_2]; this is in contrast to the inertness of the $\{Fe^{III}(NO^-)\}^7$ complex $[Cl_3Fe(NO)]^-$ [having an axial EPR spectrum with $g_\perp = 3.926$ and $g_\parallel = 2.000$ (CH_2Cl_2)] toward NO or PPh_3. These results demonstrate that both electronic structure [$\{Fe^{III}(NO^-)\}^7$, $S = {}^3/_2$] and redox-active ligands ($[RS]^-$ for $[(RS)_3Fe(NO)]^-$ and $[NO^-]$ for complex **2**) are required for the transformation of $\{Fe(NO)\}^7$ MNICs into $\{Fe(NO)_2\}^9$ DNICs.[10] When $[C_4H_7N_2][BF_4]$ (i.e., protonated 1-MeIm) was added to a THF solution of complex **3** with 1:1 stoichiometry at 0 °C, transformation of complex **3** into the complex [(1-MeIm)(ONO)Fe$(NO)_2$] (**4**) was observed and monitored by ν_{NO} IR spectroscopy; the shift in the stretching frequencies from 1704(vs) and 1774(s) cm^{-1} to 1720(vs) and 1790(s) cm^{-1} confirmed the formation of the neutral DNIC **4**. Reversibly, the formation of complex **3** was observed upon the addition of 1 equiv of [PPN][NO_2] to the THF solution of complex **4** at ambient temperature (Scheme 1c,c′).

The variable-temperature EPR spectra demonstrate that the interconversion between the neutral four-coordinate DNIC **4** and the neutral six-coordinate DNIC **5** occurred in THF (Scheme 1d,d′).[9] Consistent with the results obtained from the variable-temperature EPR spectra, the UV−vis spectrum of complex **4** displays absorptions 516, 603, and 728 nm (THF) at 303 K (Figure 3a). Upon the addition of a 100-fold excess of 1-MeIm to the THF solution of complex **4**, the absorptions 410, 546, and 900 nm at 193 K appear, indicating the complete transformation of complex **4** into complex **5** (Figure 3b). The enthalpy and entropy were calculated to be −11.0 kJ mol^{-1} and −14.2 J K^{-1} mol^{-1}, respectively, by monitoring this equilibrium reaction from 193 to 283 K in CH_2Cl_2 using UV−vis spectroscopy.

Magnetic susceptibility data of powdered samples of complexes **3**, **4**, and **5** were collected over the temperature range 2−300 K in a 1 T applied field. The net molar magnetic susceptibility (χ_M) increases from 1.210×10^{-3} cm^3 mol^{-1} at 300 K to 0.176 cm^3 mol^{-1} at 2 K for complex **3**, from 1.805×10^{-3} cm^3 mol^{-1} at 300 K to 0.061 cm^3 mol^{-1} at 2 K for complex **4**, and from 1.684×10^{-3} cm^3 mol^{-1} at 300 K to 0.173 cm^3 mol^{-1} at 2 K for complex **5** (Figures S2−S4 in the Supporting Information). The corresponding $\chi_M T$ values (0.375 cm^3 mol^{-1} K for complex **3**, 0.542 cm^3 mol^{-1} K for complex **4**, and 0.505 cm^3 mol^{-1} K for complex **5**) and effective magnetic moments ($\mu_{eff} = 1.732\mu_B$ for complex **3**, $\mu_{eff} = 2.082\mu_B$ for complex **4**, and $\mu_{eff} = 2.010\mu_B$ for complex **5**) exhibit temperature-independent magnetic behavior indicating that the ground state has one unpaired electron and $S_{total} = {}^1/_2$.

Conversion of Nitrite to Nitric Oxide Activated by $\{Fe(NO)_2\}^{10}$ DNIC 7 via a Nitrosonium-Containing Intermediate. Upon addition of 1 equiv of nitrite to a THF solution of complex **6**, the coordinated 1-MeIm of complex **6** was substituted to generate the anionic N-bound nitro-containing $\{Fe(NO)_2\}^{10}$ DNIC [PPN][(η^1-NO_2)(PPh_3)Fe$(NO)_2$] (**7**), which was characterized by IR [ν_{NO} (cm^{-1}): 1642(vs), 1693(s) (CH_2Cl_2)] and UV−vis spectroscopies along with single-crystal X-ray crystallography (Scheme 2a). In contrast to stronger electron-donating (π-donor) ligands L (L = thiolates, imidazolate) that promote ligand exchange of the $\{Fe(NO)_2\}^9$ DNIC $[(L')_2Fe(NO)_2]^-$ (L′ = phenoxide, nitrite) to generate the stable $\{Fe(NO)_2\}^9$ DNIC $[L_2Fe(NO)_2]^-$,[11] the stronger π-acceptor nitro ligand triggered ligand substitution of complex **6** to yield the stable N-bound nitro-containing $\{Fe(NO)_2\}^{10}$ DNIC **7** in the $\{Fe(NO)_2\}^{10}$ DNICs. Qualitatively, these results may indicate that the nitrite-containing $\{Fe(NO)_2\}^9$ DNICs **3**−**5** were isolated with the O-bound nitrito ligation

(10) (a) Lu, T.-T.; Chiou, S.-J.; Chen, C.-Y.; Liaw, W.-F. *Inorg. Chem.* **2006**, *45*, 8799–8806. (b) Harrop, T. C.; Song, D.; Lippard, S. J. *J. Am. Chem. Soc.* **2006**, *128*, 3528–3529.

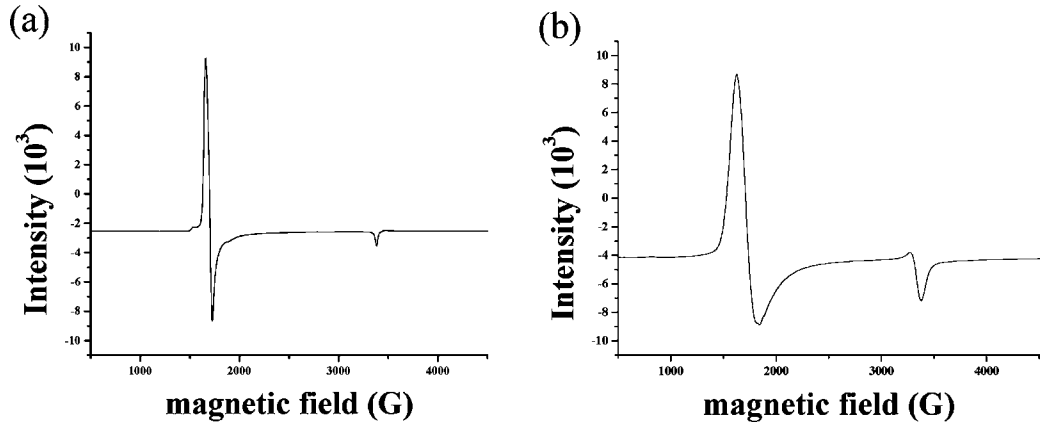

Figure 2. EPR spectra of (a) complex **2** at 4 K [$g_\perp = 3.971$, $g_\parallel = 2.000$ (CH_2Cl_2)] and (b) [PPN][$Cl_3Fe(NO)$] at 4 K [$g_\perp = 3.926$, $g_\parallel = 2.000$ (CH_2Cl_2)].

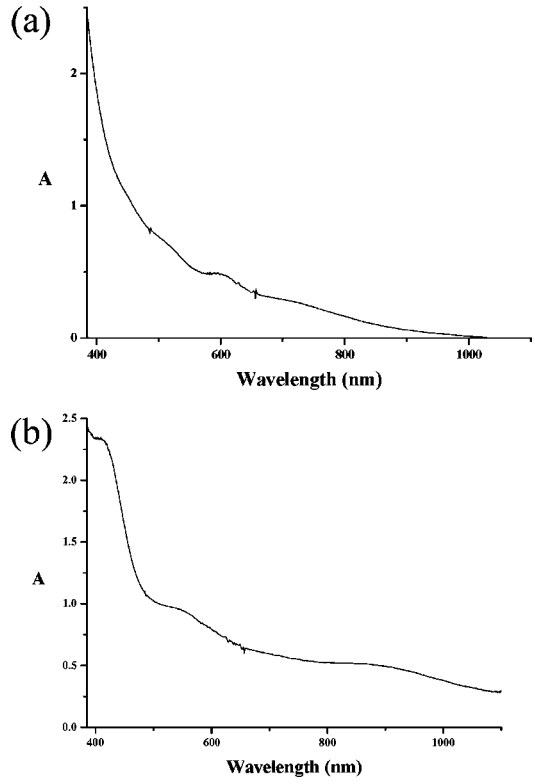

Figure 3. (a) UV−vis spectrum of complex **4** in THF at 303 K. (b) UV−vis spectrum of complex **4** in the presence of a 100-fold excess of 1-MeIm in THF at 193 K, indicating the complete transformation of complex **4** into complex **5**.

mode, in contrast to the nitrite-containing $\{Fe(NO)_2\}^{10}$ DNIC **7**, which prefers the N-bound nitro-coordinated ligand, since O-bound nitrito has been known to serve as a σ-donor ligand and N-bound nitro to act as a π-acceptor ligand.[12]

The chelating O-bound nitrito ligand in $\{Fe(NO)_2\}^9$ DNIC **5** was demonstrated to undergo PPh_3-triggered nitrite-to-nitroxyl-

Scheme 2

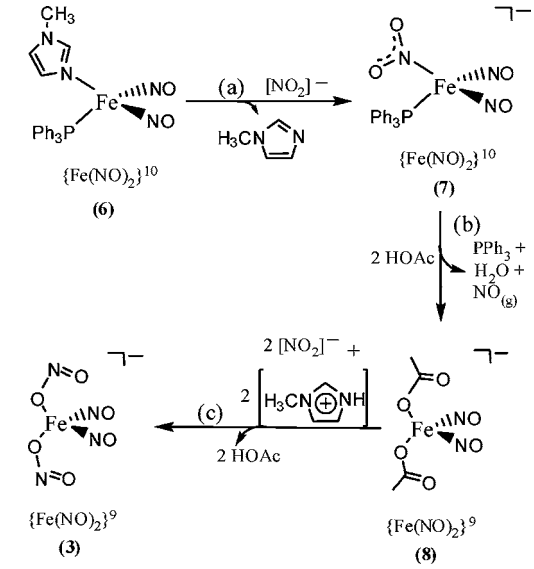

to-nitric oxide conversion accompanied by the transformation of $\{Fe(NO)_2\}^9$ DNIC **5** into $\{Fe(NO)_2\}^{10}$ DNIC **6**.[9] In order to explore the activity of the N-bound nitro ligand in $\{Fe(NO)_2\}^{10}$ DNIC **7** as a functional model for nitrite-to-nitrosonium-to-nitric oxide conversion accompanied by the transformation of $\{Fe(NO)_2\}^{10}$ DNICs into $\{Fe(NO)_2\}^9$ DNICs, protonation of complex **7** was investigated. The formation of the $\{Fe(NO)_2\}^9$ DNIC [PPN][$(OAc)_2Fe(NO)_2$] (**8**), nitric oxide, and H_2O was observed when a THF suspension of the N-bound nitro-containing $\{Fe(NO)_2\}^{10}$ DNIC **7** was treated with 2 equiv of glacial acetic acid (Scheme 2b). DNIC **8** was isolated and characterized by IR, EPR, and UV−vis spectroscopies along with single-crystal X-ray diffraction. Complex **8** in THF exhibits an isotropic EPR signal $g_{av} = 2.031$ with a well-resolved five-line hyperfine splitting ($a_{NO} = 2.15$ G) at 300 K and a rhombic pattern with principal g values of $g_1 = 2.052$, $g_2 = 2.030$, and $g_3 = 2.014$ at 77 K (Figure 4). The released nitric oxide obtained from the reaction of complex **7** and glacial acetic acid was trapped by $[PPN]_2[S_5Fe(\mu\text{-}S)_2FeS_5]$ to produce the known complex [PPN][$S_5Fe(NO)_2$].[15e] The PPh_3 byproduct was characterized by ^{31}P NMR spectroscopy [$\delta = -4.3$ ppm ($CDCl_3$)]. In isotopic experiments, reaction of complex **7** with 2 equiv of CH_3COOD in THF yielded complex **8**, NO, and D_2O. The produced DHO derived from D/H exchange between D_2O and THF was characterized by ^2H NMR spectroscopy (THF) [$\delta =$

(11) (a) Tsai, M.-C.; Tsai, F.-T.; Lu, T.-T.; Tsai, M.-L.; Wei, Y.-C.; Hsu, I.-J.; Lee, J.-F.; Liaw, W.-F. *Inorg. Chem.* **2009**, *48*, 9579–9591. (b) Huang, H.-W.; Tsou, C.-C.; Kuo, T.-S.; Liaw, W.-F. *Inorg. Chem.* **2008**, *47*, 2196–2204. (c) Tsai, F.-T.; Chiou, S.-J.; Tsai, M.-C.; Tsai, M.-L.; Huang, H.-W.; Chiang, M.-H.; Liaw, W.-F. *Inorg. Chem.* **2005**, *44*, 5872–5881.

(12) (a) Conradie, J.; Ghosh, A. *Inorg. Chem.* **2006**, *45*, 4902–4909. (b) Hitchman, M. A.; Rowbottom, G. L. *Coord. Chem. Rev.* **1982**, *42*, 55–132.

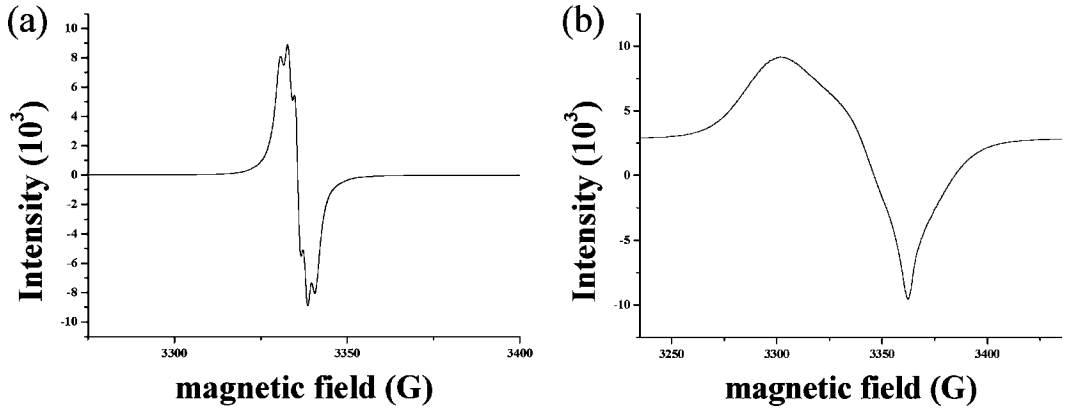

Figure 4. EPR spectra of complex **8** in THF at (a) 300 K ($g_{av} = 2.031$, $a_{NO} = 2.15$ G) and (b) 77 K ($g_1 = 2.052$, $g_2 = 2.030$, $g_3 = 2.014$, $g_{av} = 2.032$).

Scheme 3

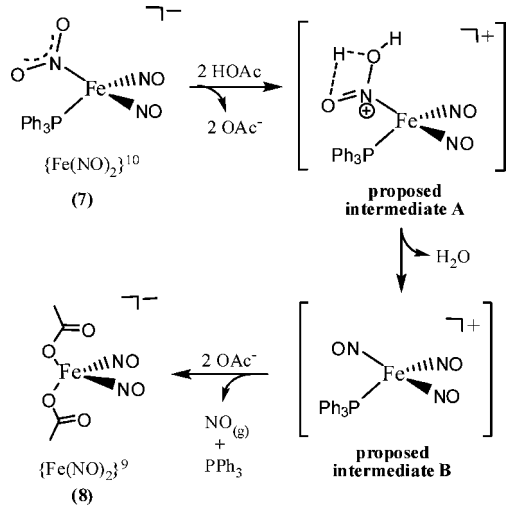

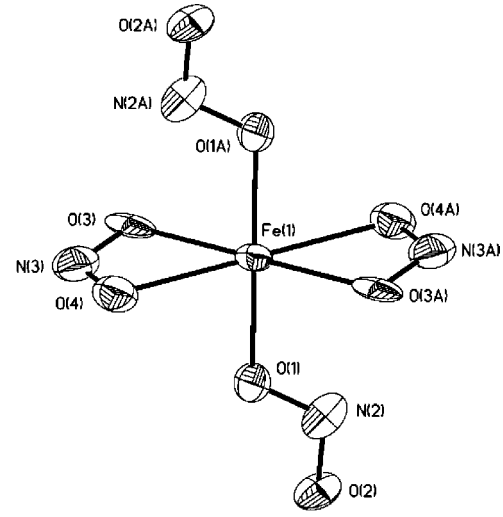

Figure 5. ORTEP drawing and atom-labeling scheme for complex **1** with thermal ellipsoids drawn at 50% probability. Selected bond lengths (Å) and angles (deg): Fe(1)−O(1), 2.077(4); Fe(1)−O(3), 2.494(9); Fe(1)−O(4), 2.218(8); N(3)−O(3), 1.215(8); N(3)−O(4), 1.477(10); N(2)−O(1), 1.268(6); N(2)−O(2), 1.235(6); O(3)−Fe(1)−O(4), 55.7(3); O(3)−N(3)−O(4), 110.2(7).

2.84 ppm (DHO) vs 5.32 ppm (CD_2Cl_2)]. To further corroborate the generation of H_2O derived from protonation of complex **7**, the reaction of complex **7** and 2 equiv of benzoic acid in C_4D_8O (3 mL) was conducted. An ^1H NMR resonance (in C_4D_8O) appearing as a broad peak at 2.54 ppm (DHO) that was derived from H/D exchange of the produced H_2O and C_4D_8O was found. The reaction sequences given in Scheme 3 reasonably account for the transformation of DNIC **7** into DNIC **8** along with byproducts NO, H_2O, and PPh_3 promoted by protonation: the reaction proceeds via nitrite protonation to yield intermediate **A**, after which dehydration affords the intermediate $[(PPh_3)(NO)Fe(NO)_2]^+$ (**B**) containing a nitrosonium-coordinated ligand (nitrite-to-nitrosonium conversion); subsequent elimination of NO(g) and concomitant coordination of acetates result in the formation of complex **8**.

The preferred formation of nitrite-containing $\{Fe(NO)_2\}^9$ DNICs via a ligand-exchange reaction may be dictated by the thermodynamic preference for stronger electron-donating ligands (electron-donating ability: $[ONO]^- > HOAc$).[11a] As shown in Scheme 2c, when a mixture of 1-MeIm and HBF_4 (1:1 molar ratio) was added into a THF/CH_3CN solution of complex **8** and [PPN][NO_2] (1:2 molar ratio) at 0 °C, the transformation of complex **8** into complex **3** was observed and monitored by ν_{NO} IR spectroscopy; the shift in the stretching frequencies from 1693(vs) and 1771(s) cm^{-1} to 1704(vs) and 1774(s) cm^{-1} confirmed the formation of DNIC **3**.

Structure. Figures 5 and 6 show thermal ellipsoid plots of complexes **1** and **2**, respectively, and selected bond lengths and bond angles are given in the captions of these figures. The iron in complex **1** is located at the center of an O_6 environment composed of two O-bound monodentate nitrito ligands and two O-bound bidentate nitrito ligands. The O(1)−Fe(1)−O(1A) bond angle in complex **1** is 180.0°. The constraint of the bidentate nitrito ligand generates an O(3)−Fe(1)−O(4) bond angle of 55.7(3)°, enforcing a severe distortion from an octahedron at the six-coordinate iron site. The most striking feature of complex **1** is the difference of 0.262(9) Å between the N(3)−O(4) and N(3)−O(3) bond lengths of the O-bound bidentate nitrito ligands, which is significantly larger than the difference of 0.004 Å between the N(3)−O(4) and N(3)−O(3) bond lengths in the known $\{Fe(NO)_2\}^9$ DNIC **5**.[9] The (Fe)O(1)−N(2) bond length of 1.268(6) Å in the monodentate O-bound nitrito ligand in complex **1** is comparable to the distal N(2)−O(2) bond length of 1.235(6) Å. The single-crystal X-ray structure of complex **2** was found to have the orthorhombic *Pbca* space group. The iron center in complex **2** adopts an octahedral geometry consisting of one NO molecule, one O-bound bidentate nitrito

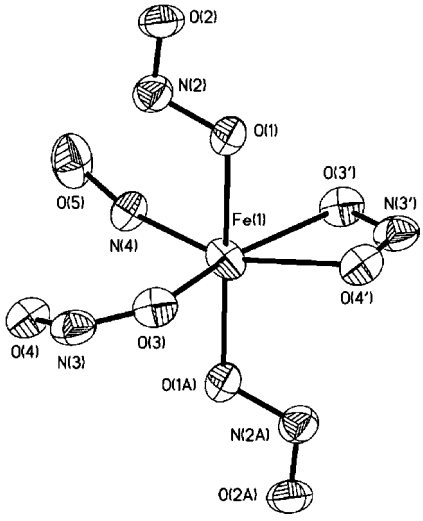

Figure 6. ORTEP drawing and atom-labeling scheme for complex **2** with thermal ellipsoids drawn at 50% probability. Selected bond lengths (Å) and angles (deg): Fe(1)−N(4), 1.906(6); Fe(1)−O(1), 2.054(3); Fe(1)−O(3), 1.987(6); Fe(1)−O(3′), 2.161(9); Fe(1)−O(4′), 2.120(7); N(4)−O(5), 1.138(9); N(2)−O(1), 1.278(4); N(2)−O(2), 1.230(5); N(3)−O(3), 1.238(11); N(3)−O(4), 1.231(10); N(3′)−O(3′), 1.265(12); N(3′)−O(4′), 1.160(12); Fe(1)−N(4)−O(5), 154.5(7); O(3′)−Fe(1)−O(4′), 57.1(3); O(3′)−N(3′)−O(4′), 115.1(10).

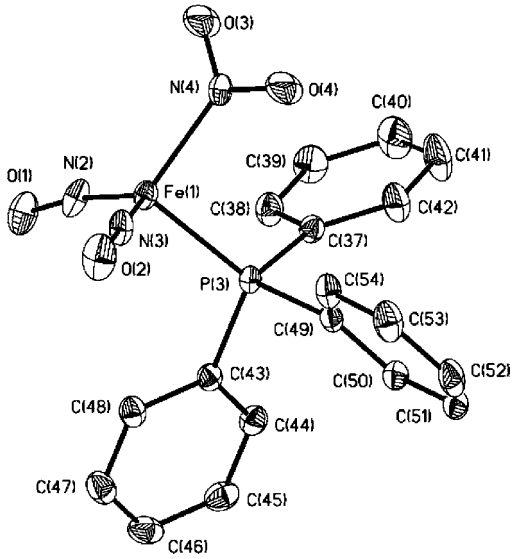

Figure 7. ORTEP drawing and atom-labeling scheme for complex **7** with thermal ellipsoids drawn at 50% probability. Selected bond lengths (Å) and angles (deg): Fe(1)−N(2), 1.6462(17); Fe(1)−N(3), 1.667(4); Fe(1)−N(4), 2.025(3); Fe(1)−P(3), 2.2483(5); N(2)−O(1), 1.202(2); N(3)−O(2), 1.210(5); N(4)−O(3), 1.208(4); N(4)−O(4), 1.222(3); Fe(1)−N(2)−O(1), 169.81(19); Fe(1)−N(3)−O(2), 174.0(4); N(4)−Fe(1)−P(3), 95.35(8).

ligand, and three O-bound monodentate nitrito ligands. The constraint of the bidentate nitrito ligand generates an O(3′)−Fe(1)−O(4′) bond angle of 57.1(3)°, enforcing a severe distortion at the six-coordinate iron site. The difference of 0.105(12) Å between the N(3′)−O(3′) and N(3′)−O(4′) bond lengths in the O-bound bidentate nitrito ligands is slightly smaller than in complex **1** [0.262(9) Å]. The N(4)−O(5) bond length of 1.138(9) Å falls in the reported range of 1.002(9)−1.193(4) Å for {Fe(NO)}^{7} MNICs.[10,13] It should be noted that the Fe(1)−N(4) bond length of

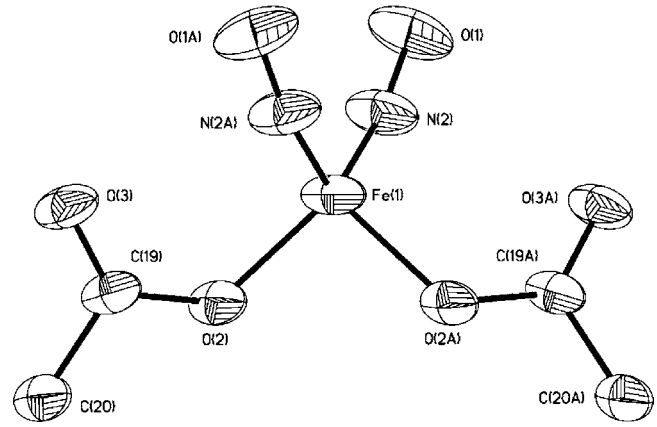

Figure 8. ORTEP drawing and atom-labeling scheme for complex **8** with thermal ellipsoids drawn at 50% probability. Selected bond lengths (Å) and angles (deg): Fe(1)−N(2), 1.689(3); N(2)−O(1), 1.178(3); Fe(1)−O(2), 1.948(2); Fe(1)−N(2)−O(1), 161.6(3); O(2)−Fe(1)−O(2A), 97.95(13).

Scheme 4

(a) {Fe(NO)$_2$}^{9} DNIC **5** coordinated by O-bound binding mode of [NO$_2$]$^-$

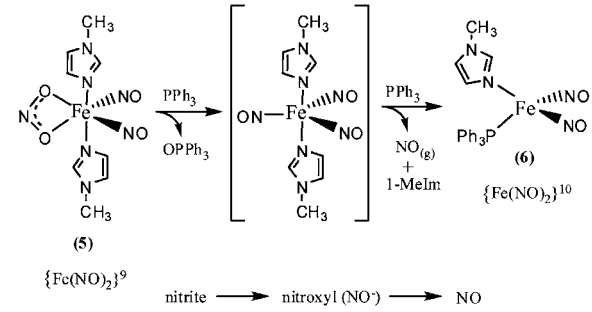

(b) {Fe(NO)$_2$}^{10} DNIC **7** coordinated by π-accepting binding mode of [NO$_2$]$^-$

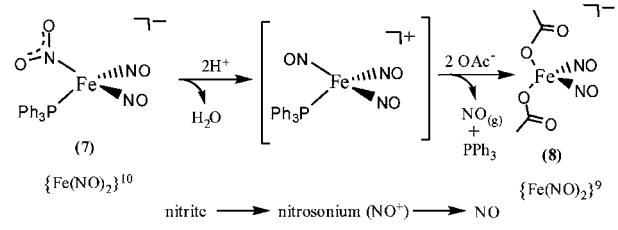

1.906(6) Å in complex **2** is significantly longer than the reported Fe−N(O) bond lengths of 1.659(6)−1.779(9) Å in {Fe(NO)}^{7} MNICs.[10,13]

The molecular structures of complexes **7** and **8** are depicted in Figures 7 and 8, respectively, and the selected bond lengths and bond angles are presented in the figure captions. The Fe(1)−N(O) bond lengths of 1.6462(17) and 1.667(4) Å in complex **7** fall in the range reported for {Fe(NO)$_2$}^{10} DNICs.[14] The N−O bond lengths of 1.202(2) and 1.210(5) Å in complex **7** are comparable to the published N−O bond lengths of 1.189(4)−1.214(6) Å for {Fe(NO)$_2$}^{10} DNICs.[14b] It should be noted that the N(4)−O(4) bond length of 1.222(3) Å in the

(13) (a) Lee, C.-M.; Hsieh, C.-H.; Dutta, A.; Lee, G.-H.; Liaw, W.-F. *J. Am. Chem. Soc.* **2003**, *125*, 11492–11493. (b) Lee, C.-M.; Chen, C.-H.; Chen, H.-W.; Hsu, J.-L.; Lee, G.-H.; Liaw, W.-F. *Inorg. Chem.* **2005**, *44*, 6670–6679.

(14) (a) Tsou, C.-C.; Lu, T.-T.; Liaw, W.-F. *J. Am. Chem. Soc.* **2007**, *129*, 12626–12627. (b) Hung, M.-C.; Tsai, M.-C.; Lee, G.-H.; Liaw, W.-F. *Inorg. Chem.* **2006**, *45*, 6041–6047.

Scheme 5

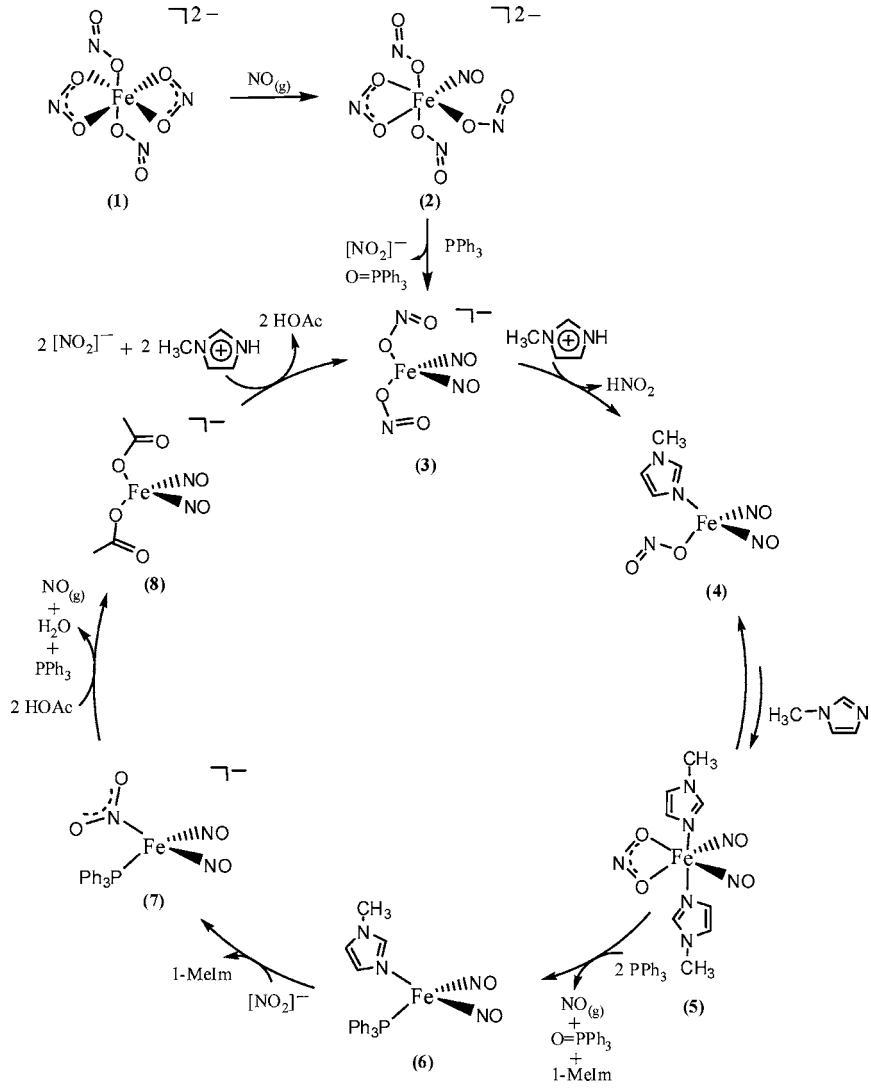

N-bound nitro ligand is comparable to the N(4)−O(3) bond length of 1.208(4) Å, in contrast to the significant difference between the N(3)−O(4) and N(3)−O(3) bond lengths of the bidentate O-bound nitrito ligand observed in complex **1**. The iron center in complex **8** exhibits a distorted tetrahedral geometry with an O(2)−Fe(1)−O(2A) bond angle of 97.95(13)°. The Fe(1)−O(2) bond length of 1.948(2) Å is longer than the average Fe−O(Ph) bond length [1.917(2) Å] in [PPN]-[$(OPh)_2Fe(NO)_2$].[11a] The Fe(1)−N(2) bond length of 1.689(3) Å falls in the range 1.661(4)−1.695(3) Å observed in anionic $\{Fe(NO)_2\}^9$ DNICs. Also, the N(2)−O(1) bond length of 1.178(3) Å is within the range 1.160(6)−1.178(3) Å observed for anionic $\{Fe(NO)_2\}^9$ DNICs.[11,14b,15]

Conclusion and Comments

Studies of the nitrite-containing DNICs and MNICs and interconversion of the nitrite-containing $\{Fe(NO)_2\}^9$ and $\{Fe(NO)_2\}^{10}$ DNICs have led to the following results (including some from the previous study[9]) related to the nitrite activation:

(1) The O-bound nitrito ligand acts as a σ-donor ligand to stabilize the $\{Fe(NO)_2\}^9$ DNICs **3**−**5**, whereas the N-bound nitro ligand in the $\{Fe(NO)_2\}^{10}$ DNIC **7** acts as a π-acceptor ligand to stabilize the electron-rich $\{Fe(NO)_2\}^{10}$ DNIC. Also, this study has shown that ligand substitution of $\{Fe(NO)_2\}^9$ DNICs is promoted by stronger π-donor ligands,[11] whereas stronger π-acceptor ligands trigger ligand exchange of the $\{Fe(NO)_2\}^{10}$ DNICs (e.g., conversion **6** into **7**).

(2) PPh_3-promoted O-atom transfer from the chelating nitrito ligand in MNIC **2** under mild conditions generates the proposed intermediate $[(ONO)_3Fe^{III}(NO^-)_2]^{2-}$, from which subsequent elimination of $[NO_2]^-$ yields $\{Fe(NO)_2\}^9$ DNIC **3**. Conclusively, both the electronic structure of the $\{Fe^{III}(NO^-)\}^7$ ($S = {}^3/_2$) core and redox-active ligands ($[RS]^-$ for $[(RS)_3Fe(NO)]^-$; $[NO^-]$ for complex **2**) in MNICs play key roles in promoting the transformation of $\{Fe(NO)\}^7$ MNIC **2** into $\{Fe(NO)_2\}^9$ DNIC **3**.[10a]

(3) (a) The nitrite-to-nitroxyl-to-nitric oxide conversion pathway is activated by the $\{Fe(NO)_2\}^9$ DNIC and accompanied by transformation of $\{Fe(NO)_2\}^9$ to $\{Fe(NO)_2\}^{10}$

(15) (a) Lu, T.-T.; Tsou, C.-C.; Huang, H.-W.; Hsu, I.-J.; Chen, J.-M.; Kuo, T.-S.; Wang, Y.; Liaw, W.-F. *Inorg. Chem.* **2008**, *47*, 6040–6050. (b) Tsai, M.-L.; Hsieh, C.-H.; Liaw, W.-F. *Inorg. Chem.* **2007**, *46*, 5110–5117. (c) Tsai, M.-L.; Liaw, W.-F. *Inorg. Chem.* **2006**, *45*, 6583–6585. (d) Chen, T.-N.; Lo, F.-C.; Tsai, M.-L.; Shih, K.-N.; Chiang, M.-H.; Lee, G.-H; Liaw, W.-F. *Inorg. Chim. Acta* **2006**, *359*, 2525–2533. (e) Tsai, M.-L.; Chen, C.-C.; Hsu, I.-J.; Ke, S.-C.; Hsieh, C.-H.; Chiang, K.-A.; Lee, G.-H.; Wang, Y.; Chen, J.-M.; Lee, J.-F.; Liaw, W.-F. *Inorg. Chem.* **2004**, *43*, 5159–5167.

(Scheme 4a). The chelating nitrito ligand in {Fe(NO)$_2$}^{9} DNIC **5** undergoes PPh_3-promoted O-atom transfer to give the proposed intermediate [(1-MeIm)$_2$(NO)Fe(NO)$_2$] with a nitroxyl-coordinated ligand (nitrite-to-nitroxyl conversion). Subsequent reductive elimination of NO(g) and the concomitant ligand substitution of 1-MeIm by PPh_3 yield {Fe(NO)$_2$}^{10} DNIC **6**. (b) The nitrite-to-nitrosonium-to-nitric oxide conversion pathway is activated by the {Fe(NO)$_2$}^{10} DNIC and accompanied by transformation of {Fe(NO)$_2$}^{10} to {Fe(NO)$_2$}^{9} (Scheme 4b). Protonation of the N-bound nitro ligand of {Fe(NO)$_2$}^{10} DNIC **7** followed by dehydration leads to the proposed intermediate [(PPh_3)(NO)Fe(NO)$_2$]$^+$ with a nitrosonium-coordinated ligand (nitrite-to-nitrosonium conversion). Subsequent elimination of NO(g) and the concomitant ligand substitution of PPh_3 by acetate yield {Fe(NO)$_2$}^{9} DNIC **8**. Obviously, the distinct electronic structures of {Fe(NO)$_2$}$^{9/10}$ motifs ({Fe(NO)$_2$}^{9} vs {Fe(NO)$_2$}^{10}) play crucial roles in modulating nitrite binding modes (O-bound chelating/monodentate nitrito as a σ donor in {Fe(NO)$_2$}^{9} DNICs vs N-bound nitro as a π acceptor for {Fe(NO)$_2$}^{10} DNICs) and regulating nitrite activation pathways (O-atom abstraction by PPh_3 leading to the intermediate containing a nitroxyl-coordinated ligand vs protonation accompanied by dehydration leading to the intermediate containing a nitrosonium-coordinated ligand) (Scheme 4). These results demonstrate that redox shuttling between {Fe(NO)$_2$}^{9} DNICs and {Fe(NO)$_2$}^{10} DNICs modulates nitrite binding modes and then triggers nitrite activation to generate nitric oxide.

Studies of nitrite activation to generate nitric oxide in biological systems are in controversy.[3] As shown in Scheme 5, study of the biomimetic reaction cycle of nitrite activation has revealed that nitrosylation of complex **1** yields nitrite-containing {Fe(NO)}^{7} MNIC **2**. Addition of 1 equiv of PPh_3 to complex **2** triggers O-atom transfer of the chelating nitrito ligand under mild conditions to yield {Fe(NO)$_2$}^{9} DNIC **3**. Protonation of complex **3** followed by 1-MeIm coordination leads to the formation of {Fe(NO)$_2$}^{9} DNIC **4**. Coordination of a second 1-MeIm to DNIC **4** triggers geometric rearrangement from the tetrahedral four-coordinate DNIC **4** to the octahedral six-coordinate DNIC **5**. The chelating nitrito ligand of {Fe(NO)$_2$}^{9} DNIC **5** undergoes PPh_3-triggered O-atom transfer to give the intermediate [(1-MeIm)$_2$(NO)Fe(NO)$_2$] containing a nitroxyl-coordinated ligand (nitrite-to-nitroxyl conversion), and subsequent reductive elimination of NO and the concomitant ligand substitution of 1-MeIm by PPh_3 yield {Fe(NO)$_2$}^{10} DNIC **6**. Ligand substitution of the coordinated 1-MeIm ligand of {Fe(NO)$_2$}^{10} DNIC **6** by nitrite generates the N-bound nitro-containing {Fe(NO)$_2$}^{10} DNIC **7**. Protonation followed by dehydration of the coordinated N-bound nitro ligand in DNIC **7** produces the intermediate [(PPh_3)(NO)Fe(NO)$_2$]$^+$ containing a nitrosonium-coordinated ligand (nitrite-to-nitrosonium conversion), and subsequent NO release and the concomitant ligand substitution of PPh_3 by acetate lead to {Fe(NO)$_2$}^{9} DNIC **8**. Protonation of acetate ligands of DNIC **8** followed by nitrite coordination regenerates DNIC **3**. This study demonstrates that the {Fe(NO)$_2$} motif plays the key role in modulating nitrite activation and delineates how imidazole participates in regulating the iron activation center. These results demonstrate that both the nonclassical six-coordinate O-bound chelating nitrito-containing {Fe(NO)$_2$}^{9} DNIC **5** and the classical four-coordinate N-bound nitro-containing {Fe(NO)$_2$}^{10} DNIC **7** may act as active centers to trigger the transformation of nitrite into nitric oxide.

The studies of complexes **1**−**8** exploring nitrite activation [nitrite-to-nitroxyl conversion (Fe−NO$^-$) or nitrite-to-nitrosonium conversion (Fe−NO$^+$)] and modulation of nitrite activation by the geometry/coordination environment of {Fe(NO)$_2$} may lend credence to the proposal that nitrite activation may occur on the {Fe(NO)$_2$} motif in biological systems (Scheme 5). Presumably, the dynamic equilibrium between DNICs **4** and **5** may play a crucial role in tuning NO homeostasis under hypoxic conditions. Also, this result may signify that nitrite-containing DNICs may act as NO/NO_2^- storage/transport species to maintain cellular NO homeostasis in biological systems.

Experimental Section

General. Manipulations, reactions, and transfers were conducted under nitrogen according to Schlenk techniques or in a glovebox (nitrogen gas). Solvents were distilled under nitrogen from appropriate drying agents (diethyl ether from CaH_2; acetonitrile from $CaH_2-P_2O_5$; methylene chloride from CaH_2; hexane and THF from sodium benzophenone) and stored in dried, N_2-filled flasks over 4 Å molecular sieves. Nitrogen was purged through these solvents before use. Solvents were transferred to the reaction vessel via stainless cannula under positive N_2 pressure. The reagents sodium nitrite (Aldrich), bis(triphenylphosphoranylidene)ammonium chloride ([PPN][Cl]) (Fluka), silver nitrite (TCI), 1-MeIm (Acros), and ferrous chloride (Strem) were used as received. The NO(g) (SanFu, 10% NO + 90% N_2) was passed through an Ascarite II column to remove higher nitrogen oxides before use. IR spectra of NO and N−O (nitrite) stretching frequencies were recorded on a PerkinElmer model Spectrum One B spectrophotometer with sealed solution cells (0.1 mm, KBr windows) or solid KBr. UV−vis spectra were recorded on a GBC Cintra 10e and Agilent 8453 spectrophotometers equipped with Unisoku cryostat. ^{1}H, ^{2}H, and ^{31}P NMR spectra were obtained on a Varian Unity-500 spectrometer. Analyses of carbon, hydrogen, and nitrogen were obtained with a CHN analyzer (Heraeus).

Preparation of [PPN]$_2$[(ONO)$_2$Fe(η^2-ONO)$_2$] (1). $FeCl_2$ (0.064 g, 0.5 mmol), $AgNO_2$ (0.154 g, 1 mmol), and [PPN][NO_2] (0.585 g, 1 mmol) were loaded into a Schlenk tube and dissolved in CH_3CN (8 mL). The reaction mixture was stirred for 1 h at 0 °C. The resulting yellow-brown solution was filtered through Celite to remove the insoluble solid (presumably AgCl). Diethyl ether (15 mL) was then added slowly to layer above the filtrate. The flask was tightly sealed and kept in the refrigerator at −20 °C for 2 weeks to yield dark-brown crystals of [PPN]$_2$[(ONO)$_2$Fe(η^2-ONO)$_2$] (**1**) (0.5 g, 38% yield) suitable for X-ray diffraction analysis. Absorption spectrum (CH_3CN) λ_{max}/nm (ε/M^{-1} cm^{-1}) (233 K): 261 (8307), 267 (9338), 274 (7622), 441 (367), 576 (186). Anal. Calcd for $C_{72}H_{60}N_6O_8P_4Fe\cdot 2H_2O$: C, 63.90; H, 4.73; N, 6.21. Found: C, 63.70; H, 4.79; N, 6.78.

Preparation of [PPN]$_2$[(NO)Fe(ONO)$_3$(η^2-ONO)] (2). A CH_3CN solution (10 mL) of complex **1** (0.395 g, 0.3 mmol) was injected with NO gas (75 mL, 10% NO + 90% N_2) at 0 °C. After the reaction solution was stirred for 30 min at 0 °C, the dark-red-brown solution was filtered to remove the insoluble solid. The dark-brown solid [PPN]$_2$[(NO)Fe(ONO)$_3$(η^2-ONO)] (**2**) (0.21 g, 51% yield) was obtained by addition of diethyl ether (∼25 mL). Dark-brown crystals suitable for X-ray diffraction analysis were obtained from a THF/CH_3CN solution of complex **2** layered with diethyl ether/hexane at −20 °C for 1 week. IR ν_{NO} (cm^{-1}): 1777 (THF), 1800 (CH_2Cl_2), 1768 (KBr). Absorption spectrum (CH_2Cl_2) λ_{max}/nm (ε/M^{-1} cm^{-1}): 247 (18706), 262 (16759), 268 (17400), 275 (15098), 456 (389), 565 (250), 721 (114). Anal. Calcd for $C_{72}H_{60}N_7O_9P_4Fe$: C, 64.14; H, 4.45; N, 7.27. Found: C, 63.83; H, 4.78; N, 7.19.

Reaction of Complex 2 and PPh_3. Complex **2** (0.150 g, 0.1 mmol) and PPh_3 (0.027 g, 0.1 mmol) were loaded into a Schlenk tube and dissolved in THF/CH_3CN (10 mL). The reaction mixture was stirred for 3 h at ambient temperature. Hexane (7 mL) was added to the reaction solution to precipitate a white solid (presumably [PPN][NO_2]). The resulting mixture was then filtered through

Celite to remove the [PPN][NO_2]. Further addition of hexane (15 mL) to the filtrate afforded the insoluble dark-red solid [PPN][$(ONO)_2Fe(NO)_2$] (**3**) [IR ν_{NO} (cm^{-1}): 1704(vs), 1774(s) (THF)] (0.051 g, 68% yield)[11a] and the upper mixture solution. The upper mixture solution was dried under vacuum to obtain light-yellow solid $OPPh_3$, which was characterized by ^{31}P NMR spectroscopy [δ = 30.4 ppm ($CDCl_3$)].

Reaction of Complex 3 and [$C_4H_7N_2$][BF_4]. To a THF solution (2 mL) of complex **3** (0.15 g, 0.2 mmol) was added a THF/CH_3CN solution of [$C_4H_7N_2$][BF_4] prepared from the reaction of 1-MeIm (16 μL, 0.2 mmol) and HBF_4 (29 μL, 0.2 mmol) at 0 °C. The reaction mixture was stirred for 1 h at 0 °C, and diethyl ether (3 mL) was then added to precipitate a white solid (presumably [PPN][BF_4]). The resulting mixture was filtered through Celite to remove the insoluble solid. Addition of a large amount of hexane (40 mL) to the filtrate led to the precipitation of the known compound [(1-MeIm)(ONO)Fe$(NO)_2$] (**4**) (0.044 g, 95% yield). IR ν_{NO} (cm^{-1}): 1729(vs), 1800(s) (MeOH).[9]

Temperature-Dependent Dynamic Equilibrium between Complexes 4 and 5 in CH_2Cl_2 Monitored by UV−Vis Spectroscopy. Complex [$(1\text{-MeIm})_2(\eta^2\text{-ONO})Fe(NO)_2$] (**5**) (0.033 g, 0.1 mmol) and 1-MeIm (0.8 mL, 10 mmol) were dissolved in CH_2Cl_2 (20 mL) at 0 °C. The diluted solution (6.25×10^{-4} M) was cooled to 183 K. The absorption at 417 nm was monitored by UV−vis spectroscopy from 193 to 283 K. The enthalpy and entropy were calculated as −11.0 kJ mol^{-1} and −14.2 J K^{-1} mol^{-1}, respectively. Complex **5**: Absorption spectrum (CH_2Cl_2) λ_{max}/nm (ε/M^{-1} cm^{-1}) (183 K): 417 (1467), 568 (719), 910 (402). Complex **4**: Absorption spectrum (CH_2Cl_2) λ_{max}/nm (ε/M^{-1} cm^{-1}) (303 K): 520 (263), 618 (140), 750 (72).

Preparation of [PPN][$(PPh_3)(\eta^1\text{-}NO_2)Fe(NO)_2$] (7). To a stirred THF solution of the complex [(PPh_3)(1-MeIm)Fe$(NO)_2$] (**6**) (0.09 g, 0.2 mmol) in an ice bath was added dropwise a CH_3CN solution of [PPN][NO_2] (0.11 g, 0.2 mmol). The reaction mixture was stirred for 1 h in the ice bath. Diethyl ether/hexane (15 mL) was then added slowly to layer above the green solution. The flask was tightly sealed and kept in the refrigerator at −20 °C for 2 weeks to yield green crystals of [PPN][$(PPh_3)(\eta^1\text{-}NO_2)Fe(NO)_2$] (**7**) (0.16 g, 80% yield) suitable for X-ray diffraction analysis. IR (cm^{-1}): 1642(vs), 1693(s) (ν_{NO}) (CH_2Cl_2); 1637(vs), 1685(s) (ν_{NO}), 1306 (ν_{O-N-O}), 1263 ($\nu_{O-^{15}N-O}$) (KBr). Absorption spectrum (CH_2Cl_2) λ_{max}/nm (ε/M^{-1} cm^{-1}): 601 (208). Anal. Calcd for $C_{54}H_{45}N_4O_4P_3Fe\cdot CH_3CN\cdot(C_2H_5)_2O$: C, 66.82; H, 5.38; N, 6.50. Found: C, 66.81; H, 4.97; N, 6.73.

Reaction of Complex 7 and 2 Equiv of Glacial Acetic Acid. A THF suspension (5 mL) of complex **7** (0.193 g, 0.2 mmol) was prepared under a N_2 atmosphere in a vial. The vial containing the THF solution of **7** was then placed in a larger vial containing a THF/MeCN solution of [PPN]$_2$[$S_5Fe(\mu\text{-}S)_2FeS_5$] (0.078 g, 0.05 mmol). The larger vial was then capped with a well-sealed septum. A THF solution of glacial acetic acid (HOAc) (24 μL, 0.4 mmol) was then added by syringe to the vial containing the THF solution of complex **7**. The solution containing complex **7** and HOAc was stirred for 12 h at room temperature. Then the resulting green solution in the larger vial was transferred to Schlenk tube and dried under vacuum. The remaining dark-green crude solid was redissolved in THF and filtered through Celite to remove the insoluble solid. Addition of hexane to the filtrate led to the precipitation of the known dark-green solid [PPN][$S_5Fe(NO)_2$] (60%), which was characterized by its IR spectrum.[15e] At the same time, the red solution produced in the small vial [ν_{NO} (cm^{-1}): 1693(vs), 1771(s) (THF)] was transferred to a Schlenk tube and then filtered through Celite to remove the insoluble solid. Hexane was added to the filtrate to separate the insoluble red solid [PPN][$(OAc)_2Fe(NO)_2$] (**8**) (0.12 g, 65% yield) and the upper solution. The upper solution was dried under vacuum to obtain the white solid PPh_3, which was characterized by ^{31}P NMR spectroscopy [δ = −4.3 ppm ($CDCl_3$)]. Red crystals suitable for X-ray diffraction analysis were obtained from a THF solution of complex **8** layered with diethyl ether/hexane at −20 °C for 1 week. IR (cm^{-1}): 1693(vs), 1771(s) (ν_{NO}), 1630(s) (ν_{CO}) (THF). Absorption spectrum (THF) λ_{max}/nm (ε/M^{-1} cm^{-1}): 507 (528), 668 (191). Anal. Calcd for $C_{40}H_{36}N_3O_6P_2Fe$: C, 62.13; H, 4.66; N, 5.44. Found: C, 61.85; H, 4.62; N, 5.29. In the isotopic experiment, to a stirred THF suspension of complex **7** (0.193 g, 0.2 mmol) in an ice bath was added a THF solution of CH_3COOD (24 μL, 0.4 mmol). The THF solvent containing DHO (produced by D/H exchange between D_2O and THF) was trapped by liquid nitrogen under vacuum. The trapped DHO in THF was identified by ^2H NMR spectroscopy [^2H NMR (THF): δ 2.84 (DHO) vs δ 5.32 (CD_2Cl_2)]. In order to further corroborate the generation of H_2O from the reaction of complex **7** and glacial acetic acid described above, the reaction of complex **7** (0.193 g, 0.2 mmol) and 2 equiv of benzoic acid (0.05 g, 0.4 mmol) in THF-d_8 (3 mL) was conducted. The formation of H_2O was identified by ^1H NMR spectroscopy. The ^1H NMR chemical shift [δ = 2.54 ppm (DHO)] was detected as a result of H/D exchange between the produced H_2O and C_4D_8O.

Reaction of Complex 8, [PPN][NO_2], and [$C_4H_7N_2$][BF_4]. To a THF suspension (2 mL) of complex **8** (0.15 g, 0.2 mmol) and [PPN][NO_2] (0.25 g, 0.4 mmol) was added a THF/CH_3CN solution of [$C_4H_7N_2$][BF_4] prepared from the reaction of 1-MeIm (33 μL, 0.4 mmol) and HBF_4 (58 μL, 0.4 mmol) at 0 °C. The reaction mixture was stirred for 1 h at 0 °C, and the resulting mixture was filtered through Celite to remove the insoluble solid (presumably [PPN][BF_4]). Addition of a large amount of hexane (40 mL) to the filtrate led to the precipitation of [PPN][$(ONO)_2Fe(NO)_2$] (**3**) (0.12 g, 85% yield). IR ν_{NO} (cm^{-1}): 1704(vs), 1774(s) (THF).

EPR Spectroscopy. X-band EPR measurements were performed using a Bruker EMX spectrometer equipped with a Bruker TE102 cavity. The microwave frequency was measured with a Hewlett-Packard 5246 L electronic counter. X-band EPR spectra of complexes **2** and [PPN][$Cl_3Fe(NO)$] in CH_2Cl_2 were recorded under microwave powers of 19.971 and 17.773 mW at frequencies of 9.485 and 9.480 GHz and a modulation amplitude of 1.60 G at 100 kHz. X-band EPR spectra of complex **8** were recorded under a microwave power of 20.020 mW at a frequency of 9.480 GHz and a modulation amplitude of 0.8 G at 100 kHz.

Magnetic Measurements. The magnetic data were recorded on a SQUID magnetometer (Quantum Design MPMS5) under a 1 T external magnetic field over the temperature range 2−300 K. The magnetic susceptibility data were corrected for temperature-independent paramagnetism (TIP, 2×10^{-4} cm^3 mol^{-1}) and for ligand diamagnetism using tabulated Pascal's constants.[16]

Crystallography. Crystallographic data and structure refinement parameters of complexes **1**, **2**, **7**, and **8** are summarized in Tables S1−S4 in the Supporting Information. Each crystal was mounted on a glass fiber and quickly coated in epoxy resin. The crystals of complexes **1**, **2**, **7**, and **8** chosen for X-ray diffraction studies had dimensions of 0.30 × 0.30 × 0.25, 0.35 × 0.28 × 0.25, 0.30 × 0.25 × 0.25, and 0.30 × 0.30 × 0.25 mm^3, respectively. Unit-cell parameters were obtained by least-squares refinement. Diffraction measurements for complexes **1**, **2**, **7**, and **8** were carried out on a Bruker X8 APEX II CCD diffractometer with graphite-monochromatized Mo Kα radiation (λ = 0.7107 Å) between 1.91 and 26.40° for **1**, 1.91 and 28.28° for **2**, 1.27 and 27.13° for **7**, and 1.98 and 26.42° for **8**. In complex **1**, the high residual electron density (Q_1 = 3.425) was localized near O(4). This was due to the thermal disorder of the chelating nitrito ligands. Examination using the PLATON program supported the orthorhombic assignment. Also, the difference (0.3015 Å) between the *a* and *c* axes is larger than their deviation (3σ = 0.0015 Å), supporting the orthorhombic assignment. Least-squares refinement of the positional and anisotropic thermal parameters of all non-

(16) (a) Bain, G. A.; Berry, J. F. *J. Chem. Educ.* **2008**, *85*, 532–536. (b) Kahn, O. *Molecular Magnetism*; VCH: New York, 1993.
(17) North, A. C. T.; Phillips, D. C.; Mathews, F. S. *Acta Crystallogr.* **1968**, *A24*, 351–359.
(18) Sheldrick, G. M. *SHELXTL: A Program for Crystal Structure Determination*; Siemens Analytical X-ray Instruments, Inc.: Madison, WI, 1994.

hydrogen atoms and fixed hydrogen atoms was based on F^2. A semiempirical method of absorption correction[17] was made for complexes **1**, **2**, **7**, and **8**. The SHELXTL[18] structure refinement program was employed.

Acknowledgment. We gratefully acknowledge financial support from the National Science Council of Taiwan. The authors thank Mr. Ting-Shen Kuo for single-crystal X-ray structure determinations and Dr. Way-Zen Lee for the variable-temperature UV−vis measurements.

Supporting Information Available: X-ray crystallographic data (CIF) from the structure determinations for [PPN]$_2$[(ONO)$_2$-Fe(η^2-ONO)$_2$](**1**),[PPN]$_2$[(ONO)$_3$Fe(NO)(η^2-ONO)](**2**),[PPN]-[(η^1-NO$_2$)(PPh$_3$)Fe(NO)$_2$] (**7**), and [PPN][(OAc)$_2$Fe(NO)$_2$] (**8**); results of magnetic measurements; and complete ref 3d. This material is available free of charge via the Internet at http://pubs.acs.org.

JA100849R